Carcinogenesis, 2021, Vol. 42, No. 12, 1449–1460

https://doi.org/10.1093/carcin/bgab101
Advance Access publication October 23, 2021
Original Article

ORIGINAL ARTICLE

DNMT3A epigenetically regulates key microRNAs involved in epithelial-to-mesenchymal transition in prostate cancer

Monica Mancini[1,†], Margherita Grasso[2,8,†], Livio Muccillo[3,†], Federica Babbio[1], Francesca Precazzini[2], Ilaria Castiglioni[1,9], Valentina Zanetti[1,10], Francesca Rizzo[4,5], Christian Pistore[1], Maria Giovanna De Marino[1], Michele Zocchi[1], Valerio Del Vescovo[2,11], Valerio Licursi[6], Giorgio Giurato[4,5], Alessandro Weisz[4,5], Paola Chiarugi[7], Lina Sabatino[3], Michela Alessandra Denti[2,*] and Ian Marc Bonapace[1,*]

[1]Department of Biotechnology and Life Sciences, University of Insubria, 21052 Busto Arsizio, VA, Italy, [2]Department of Cellular, Computational and Integrative Biology (CIBIO), University of Trento, Povo, TN, Italy, [3]Department of Sciences and Technologies, University of Sannio, 82100 Benevento, Italy, [4]Laboratory of Molecular Medicine and Genomics, Department of Medicine, Surgery and Dentistry 'Scuola Medica Salernitana', University of Salerno, 84081 Baronissi, Italy, [5]Genome Research Center for Health, c/o University of Salerno Campus of Medicine, 84081 Baronissi, SA, Italy, [6]Department of Biology and Biotechnology "Charles Darwin", "Sapienza" University of Rome, Rome, Italy and [7]Department of Biomedical, Experimental and Clinical Sciences 'Mario Serio', University of Florence, Florence, Italy [8]Present address: L.N.Age Srl, 00040 Pomezia, RM, Italy [9]Present address: Laboratory of Gene Expression and Muscular Dystrophy, San Raffaele Scientific Institute, Milan, Italy [10]Present address: ICON Plc, 20159 Milano, Italy [11]Present address: Exom Group Srl, 20124 Milano, Italy

*To whom correspondence should be addressed. Tel: +39 0331339452; Fax: +39 0332-421326; Email: ian.bonapace@uninsubria.it
Correspondence may also be addressed to Michela Alessandra Denti. Tel: +39 0461283820; Email: michela.denti@unitn.it
†These authors contributed equally to this work.

Abstract

Epithelial-to-mesenchymal transition (EMT) is involved in prostate cancer (PCa) metastatic progression, and its plasticity suggests epigenetic implications. Deregulation of DNA methyltransferases (DNMTs) and several microRNAs (miRNAs) plays a relevant role in EMT, but their interplay has not been clarified yet. In this study, we provide evidence that DNMT3A interaction with several miRNAs has a central role in an *ex vivo* EMT PCa model obtained via exposure of PC3 cells to conditioned media from cancer-associated fibroblasts. The analysis of the alterations of the miRNA profile shows that miR-200 family (miR-200a/200b/429, miR-200c/141), miR-205 and miR-203, known to modulate key EMT factors, are down-regulated and hyper-methylated at their promoters. DNMT3A (mainly isoform a) is recruited onto these miRNA promoters, coupled with the increase of H3K27me3/H3K9me3 and/or the decrease of H3K4me3/H3K36me3. Most interestingly, our results reveal the differential expression of two DNMT3A isoforms (a and b) during *ex vivo* EMT and a regulatory feedback loop between miR-429 and DNMT3A that can promote and sustain the transition towards a more mesenchymal phenotype. We demonstrate the ability of miR-429 to target *DNMT3A* 3′UTR and modulate the expression of EMT factors, in particular ZEB1. Survey of the PRAD-TCGA dataset shows that patients expressing an EMT-like signature are indeed characterized by down-regulation of the same miRNAs with a diffused hyper-methylation at miR-200c/141 and miR-200a/200b/429 promoters. Finally, we show that miR-1260a also targets DNMT3A, although it does not seem to be involved in EMT in PCa.

Received: January 12, 2021; **Revised:** August 17, 2021; **Accepted:** October 21, 2021

Abbreviations

CM-CAF	conditioned media from cancer-associated fibroblast
EMT	epithelial-to-mesenchymal transition
MET	mesenchymal-to-epithelial transition
PCa	prostate cancer

Introduction

Prostate cancer (PCa) is the most diagnosed cancer among men and the third/second leading cause of cancer-related deaths in Europe/USA, respectively (1,2). Current treatments for primary prostatic tumour involve radical prostatectomy, radiotherapy and androgen deprivation therapy (3). However, after an initial response, patients become refractory to androgen deprivation therapy, developing castration-resistant PCa which frequently leads to metastasis and eventually to death (3). Epithelial-to-mesenchymal transition (EMT) has been shown to be a relevant process to castration-resistant PCa (4). For the transition to a complete mesenchymal state, EMT requires intermediate steps, which define metastable or stable phenotypes that depend on the persistence of EMT promoting signals (5). This plasticity suggests that the epigenetic landscape is implicated in the transition dynamics (6).

Altered DNA methylation patterns are early and consistent molecular changes of human tumours (7–10), contributing to several aspects of PCa progression (11,12). DNA methyltransferases (DNMTs) (13) and UHRF1, a reader/writer of histone marks required for proper localization of DNMT1 (14), have a central role in epigenetic gene regulation: DNMT1/UHRF1 are involved in the methylation maintenance of newly synthesized DNA strands following replication; DNMT3A and 3B are responsible for *de novo* DNA methylation at selected loci (15). DNMTs have been found to be deregulated in several tumours (10,16) and their expression and activity are elevated in prostate tumour models, as well as in androgen-resistant PCa cell lines (17,18). We have recently shown that, in an *ex vivo* model of EMT, conditioned media from patient-derived cancer-associated fibroblasts (CM-CAFs) down-regulates DNMT1/3B and UHRF1 in androgen-resistant PC3 cells, but not in androgen-responsive LNCaP cells (6). In our model, DNMT3A is pivotal: this methyltransferase is not repressed during the transition and is required for EMT by methylating the promoters of key epithelial factors, such as CDH1. These results underline the plasticity of the epigenetic regulation in sustaining and promoting cancer processes.

MicroRNAs (miRNAs) are endogenous non-coding short single-stranded RNAs that negatively regulate gene expression at the post-transcriptional level, either by degrading or inhibiting translation of the target mRNA (19). Deregulation of miRNA expression profile is associated with numerous human tumours, including PCa (20,21); they act as onco-miRNA or tumour suppressors miRNA depending on their target genes (22). Among the latter, the miR-29 family regulates DNMT3A expression in several tissues (23) and during EMT (6). Genomic rearrangements, hyper-methylation of CpG island-containing promoters or transcriptional deregulation mechanisms can alter the expression of miRNAs, linking them to the initiation/promotion of the neoplastic process (24–26). Several miRNAs are known to target EMT factors and reported to be markedly down-regulated during PCa progression, contributing to the mesenchymal phenotype. Re-expression of miR-203, miR-205 and miR-29b is known to restore the epithelial phenotype in PCa cell lines by negatively regulating EMT factors; the transcriptional repressor ZEB1 controls miR-200 family expression in breast cancer (24,27–30) and is a target of the same miRNA family (31,32).

To better clarify the role of DNMT3A in EMT, we investigated its interplay with different miRNAs in castration-resistant PCa, and their link to the EMT program associated with permanent changes in DNA methylation and expression of miRNAs (6).

Materials and methods

Cell cultures

Human PCa cell lines, PC3 (RRID:CVCL_0035) and LNCaP (RRID:CVCL_1379), were obtained from American Type Culture Collection (ATCC, Manassas, VA) in 2016 and cultured following the instructions of the company. All were authenticated using short tandem repeat profiling by ATCC, propagated, expanded and frozen immediately. Revived cells were utilized within 10–12 passages (not exceeding a period of 3 months) and regularly tested for mycoplasma contamination (N-GARDE Mycoplasma PCR Reagent set, EuroClone, Milan, IT). Both cell lines were cultured in RPMI 1640 (EuroClone) supplemented with 10% heat-inactivated fetal bovine serum (EuroClone), 2 mM glutamine and 100 U/ml penicillin/streptomycin (EuroClone).

Ex vivo EMT induction

EMT induction was performed exposing PC3 cells for 72 h to CM-CAFs or benign hyperplastic fibroblasts (CM-HPFs, control), following the published protocol (6).

Western blot analysis

Whole cell extracts were separated on 8–14% SDS–PAGE gels (Bio-Rad), and transferred to nitrocellulose membranes, then incubated with primary antibodies: DNMT3A (Active Motif, Carlsbad, CA), DNMT3A2 (Merck Millipore, Burlington, MA), E-CAD and N-CAD (Novus Biological, Littleton, CO), VIM (GeneTex, Irvine, CA) and ZEB1 (Cell Signaling Technology, Danvers, MA). Chemiluminescence reactions on secondary antimouse and antirabbit antibodies (Jackson ImmunoResearch Laboratories, West Grove, PA) was detected using ECL western blotting reagents (GE Healthcare Amersham, Chicago, IL). Equal loading was checked using GAPDH (Merk Millipore).

RNA sequencing and genome-wide DNA methylation analysis

Analysis of RNA sequencing and genome-wide DNA methylation was performed on previously published experiments (6), respectively, using HiSeq2500 platform (Illumina, San Diego, CA) with a coverage of >70 million sequence reads per sample and HumanMethylation 450 K BeadChip (Illumina), which covers 21 231 (99%) RefSeq genes. For small RNA sequencing, 1 µg of total RNA was used for indexed sequencing library preparation with a TruSeq small RNA Sample Prep Kit (Illumina) and sequenced on HiSeq1500 (Illumina) for 50 cycles.

Chromatin immunoprecipitation analysis

Chromatin immunoprecipitation was performed as previously published (6). Briefly, cells were treated with 1% formaldehyde, then 0.125 M glycine was added. The cells were collected in phosphate-buffered saline, re-suspended in lysis buffer and sonicated (BRANSON S250 digital sonicator, Branson, Danbury, CT). Pre-cleared chromatin was quantified using Qubit (dsDNA BR Assay Kit, Life Technologies); 2 µg chromatin was incubated overnight at 4°C with anti-IgG (Santa Cruz Biotechnology, Dallas, TX), anti-DNMT1, -DNMT3A, -DNMT3B, and anti-H3K9me3, -H3K27me3, -H3K4me3 and -H3K36me3 (all Active Motif). Ten percent of the total lysate was used for input control. DNA was extracted with the Chromatin IP DNA extraction kit (Active Motif) following the manufacturer protocol. Immunoprecipitation products were amplified using iTAq Polymerase (Bio-Rad, Hercules, CA) and specific primers (Supplementary Table 1B, available at *Carcinogenesis* Online).

PRAD-TCGA dataset analysis

A primary prostate adenocarcinoma (PRAD) dataset of 494 patients retrieved from of The Cancer Genome Atlas (TCGA) consortium was enquired (https://gdc-portal.nci.nih.gov). IlluminaHiSeq mRNA-Seq

expression was used to classify patients presenting EMT or mesenchymal-to-epithelial transition (MET) features. Each patient was assigned a reward or penalty score for each EMT/MET gene considered. EMT-like phenotype was defined as high levels (>Q3 or Q4, Q = quartile) of EMT genes (ZEB1, VIM, SMO, SHH, LGR5 and HEY) and low levels (<Q1 or Q2) of MET genes (CDH1, GRHL2, OVOL1/2 and ESPR1); MET-like phenotype displayed the opposite signature. Reward scores were assigned for each gene when the above-mentioned conditions were met, and penalty scores were assigned when they were disregarded. Only patients with resulting positive scores for EMT or MET were chosen, assigned to EMT-like or MET-like subgroup (47 and 40 cases, respectively) and subsequently analysed by comparing cytosines DNA methylation (Illumina, HumanMethylation 450K array) and the smallRNA-Seq expression (IlluminaHiSeq) with differentially expressed (DE) miRNAs from PC3 cell lines. The heatmaps illustrated in Figures 1B and 3 were obtained using the publicly available software Morpheus (https://software.broadinstitute.org/morpheus/) and the 'One minus Pearson correlation' as miRNAs hierarchical clustering algorithm.

miRNA target prediction

Bioinformatic tools were used to identify miRNAs predicted to target *DNMT3A*-3′UTR: http://mirdb.org (33); http://www.targetscan.org (34); http://mirna.imbb.forth.gr (35) and http://comirnet.di.uniba.it:8080/ (36). Bioinformatic analyses of transcript accessibility and binding strength calculation were performed with PITA (https://genie.weizmann.ac.il/pubs/mir07/mir07_prediction.html) (37) to predict the presence of target sites for miRNAs on *DNMT3A*-3′UTR. The hybridization minimum free energy (mfe) for miRNAs' binding was calculated with RNAhybrid (https://bibiserv.cebitec.uni-bielefeld.de/rnahybrid/) (38).

RT-qPCR

Total RNA was extracted from cells using Trizol (Invitrogen, Waltham, MA) and treated with Turbo DNA-free™ Kit (Applied Biosystem, Waltham, MA). For miRNA analysis, RNA was reverse-transcribed using TaqMan®v MicroRNA Reverse Transcription Kit (Applied Biosystem) and miRNAs were measured following the TaqMan® MicroRNA Assays (Applied Biosystem) protocol: has-miR-200b (ID: 002251), has-miR429 (ID: 001024), hsa-miR-1260a (ID: 002896), hsa-miR-29a (ID: 002112) and hsa-miR-29b (ID: 000413). U48 (RNU48, ID: 001006) was used as control. Real-time PCR reactions were carried out on a CFX Connect (Bio-Rad) using Fast Start TaqMan probe Master (Roche Life Science, Penzberg, DE). For quantitative mRNA analysis, 1 µg of total RNA was reverse-transcribed using SuperScript III RT (Invitrogen) with oligo-dT primer according to manufacturer's instructions. Real-time PCR were performed with 1X iQ™SYBR Green Supermix (Bio-Rad) as described previously (6). Levels of miRNAs or mRNAs expression were determined by Gene Expression Analysis for iCycler iQ Real-Time PCR Detection System v1.10 (Bio-Rad) according to the $2^{-\Delta\Delta Ct}$ method. Primers (Supplementary Table 1A, available at *Carcinogenesis* Online; previous publication (6)) were designed with Primer3 (http://primer3.ut.ee/) and tested against public databases (NBLAST).

Dual-luciferase reporter assay

To generate the pGL4.13[luc2/SV40]-*DNMT3A3′UTR* vector (*DNMT3A*-3′UTR), the intact *DNMT3A*-3′UTR sequence (NM_175629, 1248nt) was amplified and cloned into Firefly luciferase expressing pGL4.13[luc2/SV40] reporter vector (Promega Corporation, Madison, WI) using *FseI* restriction site. To generate the pGL4.13[luc2/SV40]-*DNMT3AΔ1260a*-3′UTR (Δ1260a_1, Δ1260a_2 and Δ1260a_1_2), the wild-type *DNMT3A*-3′UTR plasmid was used as template. Mutated constructs were created using Quick-Change II XL Site-Directed Mutagenesis Kit (Stratagene, CA), according to the manufacturer's protocol, with two complementary primers carrying the desired mutation (Supplementary Table 1A, available at *Carcinogenesis* Online). The correct mutagenesis was verified by automated Sanger DNA sequencing (BMR Genomics, Padova, IT). RegRNA (http://regrna.mbc.nctu.edu.tw/) and UTRscan (http://itbtools.ba.itb.cnr.it/utrscan) were used to exclude creation of novel binding sites or regulatory elements. The miRNA constitutive-expression cassettes for miR-429, miR-1260a, miR-608 (negative control) and miR-29a (positive control) were generated by amplification of human genomic DNA (#G1471 Promega) with PCR (primers in Supplementary Table 1A, available at *Carcinogenesis* Online). The genomic fragments containing the pre-miRNA were cloned in the BglII and XhoI sites of the psiUx plasmid (39). The same psiUx plasmid (40) was transfected in parallel as an additional negative control ('empty plasmid'). PC3 cells were seeded and transfected at 60–70% confluence using FuGENE® HD Transfection Reagent (Promega) with 50 ng of the pGL4.13 constructs containing *DNMT3A*-3′UTR wild type or mutants and 450 ng of miRNA-overexpressing plasmids. To normalize Firefly luciferase activity, a vector containing the cDNA encoding Renilla luciferase (Rluc) was co-transfected (50 ng). Twenty-four hours after transfection, cells were washed with phosphate-buffered saline and lysed with Passive Lysis Buffer (Promega); Renilla and Firefly luciferase activity were measured using the Dual-Luciferase Assay System (Promega) in the Infinite® M200 (Tecan) plate reader.

Transfection of miRNA mimics and inhibitor LNAs

PC3 cells were seeded and transfected after 24 h with mimic oligos (30 pmol miScript miRNA Mimic, QIAGEN, Hilden, DE, cat. n. 339173: miR-29a n. MSY0000086, miR-429 n. YM00472516, miR-1260a n. MSY0005911, AllStars n. 10027280) using Lipofectamine RNAiMax (Invitrogen), according to the manufacturer's recommendations. LNCaP cells were seeded and transfected after 24 h with LNA (Locked Nucleic Acids) inhibitors (30 pMol miRCURY LNA™ miRNA Inhibitor, QIAGEN, cat n. 339121: Scramble ID: YI00199006, LNA-429 ID: YI04101290, LNA-1260a ID: YI04103217) using Lipofectamine RNAiMax (Invitrogen) transfection reagent, according to the manufacturers' protocol. Cells were harvested at different times depending on the specific assay.

Cell proliferation and wound-healing assays

PC3 and LNCaP cells were transfected as reported above. Starting 3 days after transfection cells were harvested and counted every 24 h to evaluate cell growth. Simultaneously, a wound was created and observed using an Olympus BX81-inverted microscope. Images were taken by a UPlanFl ×10 objective at regular intervals over the 24–48 h course and acquired by a colour CCD camera (MicroPublisher 5.0) and the Qcapture pro software (Qimaging, Surrey, British Columbia, Canada). Precise positioning of the samples for image acquisition was achieved by a motorized stage system (Optiscan II, Prior scientific instruments, Cambridge, UK). Images were analysed using imageJ (https://imagej.nih.gov/ij/) or Photoshop (Adobe); cell migration distance was determined by measuring the width of the wound and the cell-free area, normalized at each time point to the control.

miRNA microarrays

100 ng of total RNA samples was processed and hybridized to Human miRNA V2 Microarray 8 × 15K (G4470B, Agilent Technologies) using the miRNA Microarray System labelling kit V2 (Agilent 5190-0456), according to the manufacturer's instructions. Hybridized microarray slides were scanned with an Agilent DNA Microarray Scanner G2505C and data were analysed with the Agilent ScanControl version 8.1.3 software. The scanned TIFF images were background corrected using the Agilent Feature Extraction Software version 10.7.7.1. The raw data were normalized to the 75th percentile signal intensity as recommended by the vendor. After normalization all negative signal values were replaced by 0.01 and the values from multiple replicate spots for each miRNA were summarized as median signals which were used subsequently for statistical analyses. The pairwise Welch's *T*-test was used to identify significantly deregulated miRNAs. The significance thresholds in Welch's *T*-test were set to $P < 0.05$, $|FC|>3$ and a mean signal of all samples >50th percentile. Statistical and hierarchical clustering analyses were done with the ArrayTrack Software (41).

Data analysis

Results are presented as mean ± SD of at least three independent biological and technical replicates. Statistical tests for each experiment are indicated in the figure legends. *P* values ≤0.05 were considered statistically significant (*$P \le 0.05$, **$P \le 0.01$, ***$P \le 0.001$, ****$P \le 0.0001$).

Results

Comprehensive profile of miRNA alterations during CM-CAF induced EMT in PCa cells

Several miRNAs are known to be involved in EMT and markedly up- or down-regulated during PCa progression, through

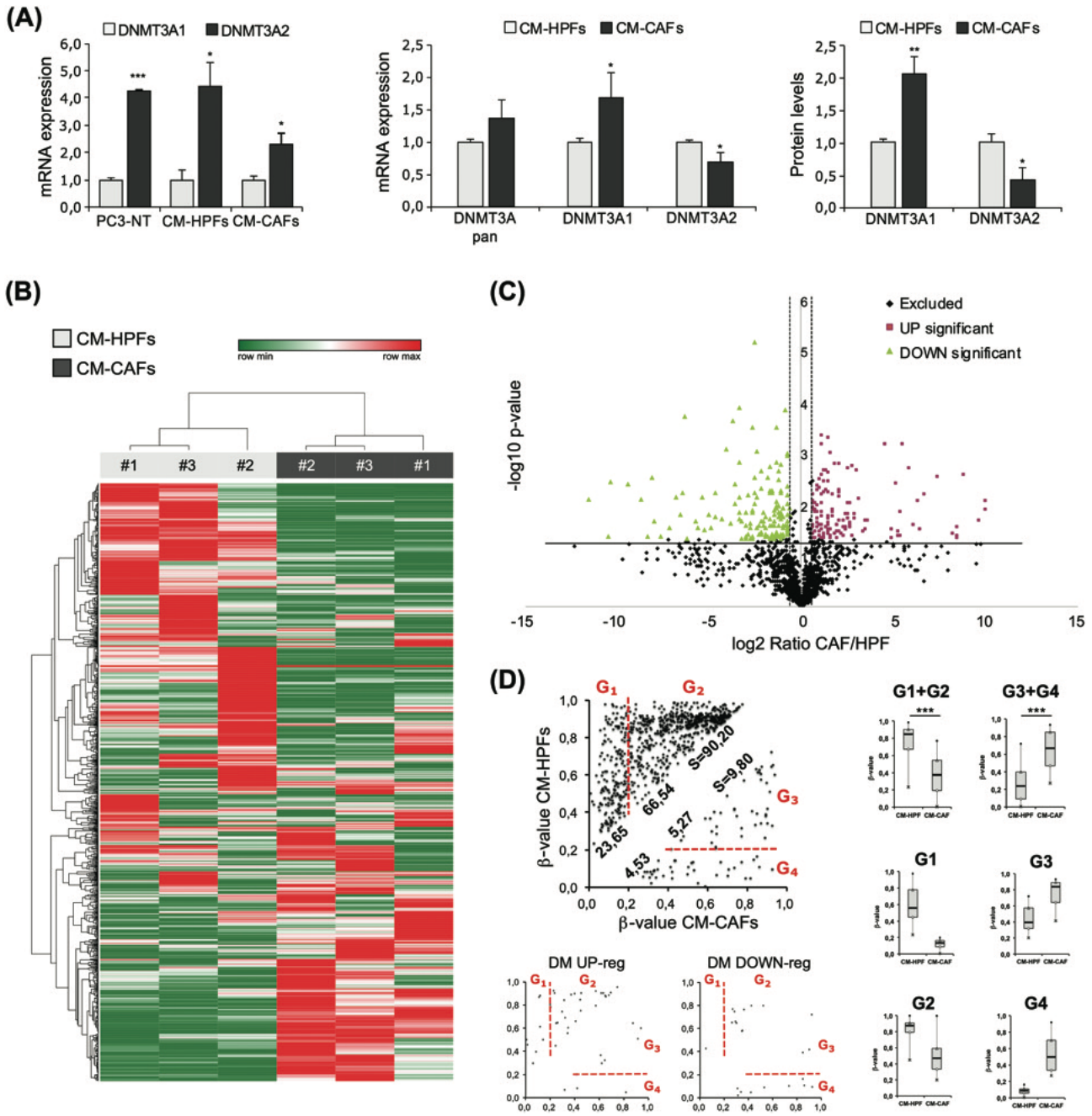

Figure 1. Analysis of DNMT3A variants and miRNAs transcription/DNA methylation profiling during *ex vivo* EMT. (**A**) Alteration of mRNA and protein levels of DNMT3A variants following EMT induction. DNMT3A variant 1 (DNMT3A1, isoform a) and variant 2 (DNMT3A2, isoform b) were analysed by qPCR (together with DNMT3A pan, assessing all known variants) and western blot in CM-HPFs and CM-CAFs PC3 cells (6). (**B** and **C**) Alteration of miRNA transcription profile following EMT induction. Heatmap (B) and volcano plot (C) of the RNA-Seq analysis (P_{adj} ≤0.05 and FC ≥1.5; ≤–1.5) of miRNAs during EMT (CM-CAFs versus CM-HPFs). The results presented in B are the average of three independent biological experiments. The P_{adj} value is computed performing the Benjamini–Hochberg test. (**D**) Alteration of miRNA promoter methylation following EMT induction. The scatter plot shows the distribution during EMT of hyper-methylated (Δβ-value ≥0.2; lower triangle) and hypo-methylated (Δβ-value ≤–0.2; upper triangle) cytosines of the DE and DM miRNAs. The scatter plot is subdivided into four gates (G1, G2, G3 and G4). G1: cytosines strongly hypo-methylated, up to complete demethylation (β-values not exceeding 0.2 in CM-CAFs); G2: hypo-methylated cytosines that achieved β-values >0.2 in CM-CAFs; G3: hyper-methylated cytosines with β-values >0.2 in CM-HPFs; G4: nearly unmethylated cytosines becoming hyper- or *de novo* methylated during EMT. The DM up- (upper part) and down- (lower part) regulated miRNAs are shown separately. On the right, box plots of the cytosine methylation variations during EMT in DE and DM miRNAs. G1 + G2: all hypo-methylated cytosines; G1: G1-gated cytosines; G2: G2-gated cytosines; G3 + G4: all hyper-methylated cytosines; G3: G3-gated cytosines. The *P* value is calculated by Mann–Whitney *U*-test (*P ≤0.05, **P ≤0.01, ***P ≤0.001, ****P ≤0.0001).

the regulatory activity of transcriptional factors such as ZEB1 or the hyper/hypo-methylation of their promoter regions (24,29). We recently reported that DNMT1, DNMT3B and UHRF1 are de-regulated in PC3 cells undergoing EMT mediated by exposure to CM-CAFs, but not in PC3 CM-HPFs (6). DNMT3A protein levels are the only slightly up-regulated, and DNMT3A-dependent alterations in DNA methylation are pivotal for the transition.

Given these published results, we sought to obtain the comprehensive profile of epigenetic alterations following EMT induction; in first instance, we investigated the mechanisms

transcriptionally regulating DNMT3A in our model, focussing on its promoter sequence. We previously demonstrated the selective methylation of DNMT3A variant 2 promoter (DNMT3A2, corresponding to isoform b) in CM-CAFs compared with CM-HPFs (6). In Figure 1A (left panel), mRNA analysis shows higher levels of DNMT3A2, compared with DNMT3A1, in non-treated (NT) PC3 cells, CM-HPF and CM-CAF. Despite the persistence of high levels of DNMT3A2 in all conditions, we observed that exposure to CM-CAF resulted in significant increase of DNMT3A1 (variant 1–3, isoform a) and decrease of DNMT3A2 (Figure 1A, central panel), which contribute to the slight (non-significant) increase of the DNMT3A (pan) total levels observed, as reported in our previous publication (6). At the protein level, we observed an even more marked shift between the two isoforms (Figure 1A, right panel, and Supplementary Figure 1A, available at *Carcinogenesis* Online).

Focussing on the effects of *ex vivo* EMT on the miRNome, we evaluated miRNA changes through RNA Sequencing and Methylation array. A total of 1276 miRNAs were detected in the two conditions. Compared with CM-HPF, CM-CAF induces in PC3 cells the deregulation of 302 miRNAs (DE, *P* value <0.05), as illustrated in Figures 1B and C. Among these, 284 showed fold change (FC) ≥1.5 or ≤–1.5 (Supplementary Table 2A and B, available at *Carcinogenesis* Online). By analysing the DE miRNAs subsets, we recognized numerous miRNAs involved in the regulation of EMT pivotal players: in particular, the miR-200 family (miR-200a/200b/429, miR-200c/141), miR-205 and miR-203.

To investigate whether miRNAs deregulation was dependent on DNA methylation variations, we analysed the previously obtained Illumina HumanMethylation 450 K BeadChip data from PC3 CM-CAFs/CM-HPFs (6). DE and differentially methylated (DM, with Δβ-value ≥0.2 or ≤–0.2 and FDR ≤0.05) miRNAs were classified as DM up-regulated and DM down-regulated (Figure 1D). We graphically divided the DM-5meC into four gates (G1, G2, G3 and G4) as previously reported (Figure 1D, see legend for definitions) (6). Around 90% of the DM cytosines were hypo-methylated (G1 + G2 gated), while only 4.5% were G4 gated, corresponding to cytosines with a β-value <0.2 in CM-HPFs and >0.2 in CM-CAFs, and therefore *de novo* methylated (G4 plots, Figure 1D).

These results demonstrate that in PC3 cells EMT induction, mediated by microenvironmental stimuli, is associated with a switch in DNMT3A isoforms and strong transcriptional and epigenetic alterations of the miRNome.

Recruitment of DNMT3A to the promoters of miR-200a/200b/429, -203 and -205a, and of miR-200c/141 during EMT

In order to investigate the role of DNMT3A (especially isoform a, significantly increased in our model) in the alteration of the miRNA profile in our *ex vivo* model, we focussed our analysis on the hyper- and *de novo*-methylated cytosines (G3 + G4 gated). We observed that the DM cytosines of miR-203 and miR-205 promoters, together with those of miR-200a/200b/429, are clustered in G4 gate in our experimental setting (CM-HPF versus CM-CAF β-values, Figure 2A–C, left panels). For the methylation analysis of miR-200a/200b/429, we surveyed the genomic region extending 5000–2000 bp upstream of the coding sequence recognized as the true promoter sequence (30). miR-200c and miR-141, known to be repressed by DNA methylation in PCa (42), instead were already hyper-methylated in PC3 CM-HPFs (β-value: >0.8); only one cytosine of the promoter region showed a slight hyper-methylation (Figure 2D, left).

The direct involvement of DNMT3A in the observed hyper-methylation was assessed through chromatin immunoprecipitation. Analysis of the promoter region of miR-200a/200b/429, -203, -205a and miR-200c/141 highlighted the recruitment of DNMT3A on all promoters only in CM-CAFs. DNMT1 was also recruited in CM-CAFs, with the likely function to maintain the newly deposited methylation marks (Figure 2, right panels, and Supplementary Figure 1B, available at *Carcinogenesis* Online). Noticeably, DNMT1 was already recruited to miR-200c/141 promoter in CM-HPFs, in line with its established methylated status. A switch between DNMT3A and 3B during EMT was observed on this promoter, supporting the role of the former methyltransferase through the process (Figure 2D). DNA hyper-methylation is associated with the appearance of repressive histone modifications, H3K27me3 and H3K9me3, and/or the decrease of activating histone modifications, H3K4me3 and H3K36me3 (Figure 2, right panels), reinforcing the repressive status of these promoters.

Investigation of specific promoter regions thus shows that DNMT3A is directly involved in the regulation of miRNAs with key roles in the EMT, further highlighting and confirming the role of this DNMT in our model.

miRNome alterations in PRAD-TCGA dataset patients displaying an EMT signature

Our *ex vivo* results on miRNome alteration were confirmed *in vivo* by analysing the PRAD-TCGA dataset, crossing the miRNA expression data with the DNA methylation profile. To select for the patients displaying opposite mesenchymal phenotype, we assigned to each sample a signature: EMT-like, defined as patients presenting high expression of EMT genes and low expression of MET genes, or MET-like, displaying the opposite pattern of expression (details in Materials and methods; Figure 3). Clustering the patients through this categorization reduced their number to 87, 40 of which presented a MET profile and the remaining 47 an EMT signature. Expression and DNA methylation of the previously identified miRNAs were evaluated in our two clusters and showed a tight correlation with expression of EMT/MET factors (Figure 3).

In particular, miR-200c and miR-141 expression inversely correlates with ZEB1 (black boxed samples), in agreement with previous evidence (30), and directly correlates with GRHL2 (the regulator of ZEB1); the promoter regions of these two miRNAs are hyper-methylated in EMT compared with MET cases (red boxed samples). miR-200a, -200b and -429 display the same correlation in both expression profile and DNA methylation (when considering the true promoter region of the polycistronic pri-miRNA transcript, as for chromatin immunoprecipitation experiments), except for a cluster of cases in MET patients where we observe methylation of the promoter and very low expression of the miRNA (red, methylation and black, expression, boxed samples). Conversely, expression of miR-203 coherently correlates with EMT/MET genes expression, but not with the level of promoter methylation. miR-205 expression does not show a significant correlation with EMT/MET mRNA levels *in vivo*. Expression analysis also shows that DNMT3A (pan) levels do not significantly differ in the two categories, recalling the importance of the experimentally observed isoform switch during the transition between the epithelial and the mesenchymal status.

These results show that the methylation status of miRNA promoters strongly relates DNA methylation and miRNA expression of miR-200c/141 and miR-200b/200c/429 in the EMT/MET TCGA samples of PCa, supporting our *in vitro* results. They also confirm the relevance of the inverse correlation between ZEB1 and miRNAs of the 200 family in EMT.

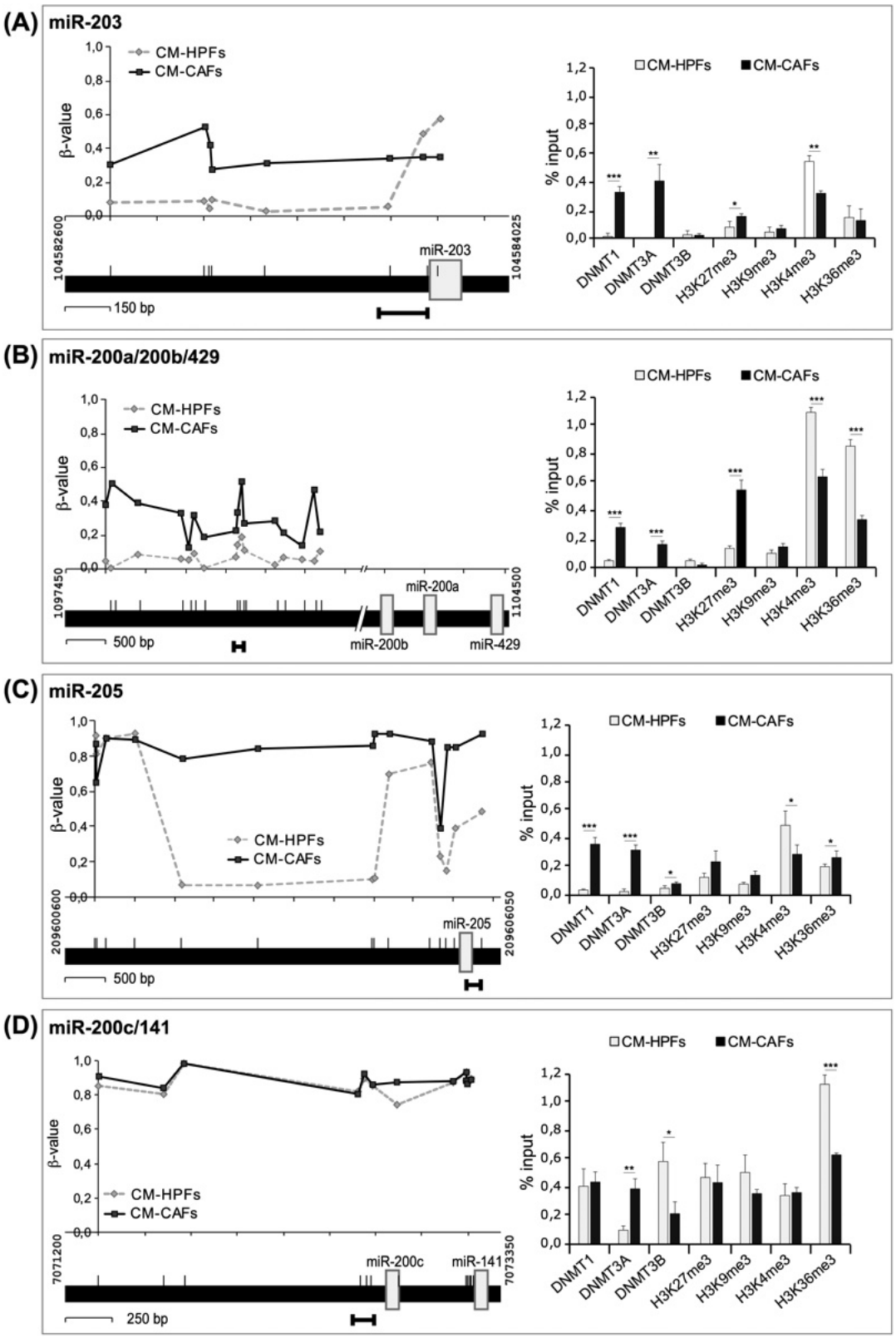

Figure 2. Analysis of DNMT3A recruitment to specific miRNA promoters during *ex vivo* EMT. (**A–D**, left) miRNA promoter structure and cytosine methylation analysis. Methylation levels were obtained through Illumina 450k array, as previously shown: miR-203 (A), miR-200b/200a/429 (B), miR-205a (C) and miR-200c/141 (D) promoter status were evaluated after exposure to CM-HPFs and CM-CAFs. The position of the different analysed cytosines is reported in the cartoons of the four promoter regions, together with the related sites analysed by ChIP. Nucleotide number and position on the chromosomes refer to the reference GRCh37.p13 primary assembly (annotation release 105.20201022). (A–D, right) Evaluation of the epigenetic status of miRNA promoters. miR-203 (A), miR-200a/200b/429 (B), miR-205a (C) and miR-200c/141 (D) promoters were investigated through ChIP experiments performed against DNA methyltransferases (DNMT1, -3A and -3B) and the indicated histone modifications (H3K9me3, H3K27me3, H3K4me3 and H3K36me3). Bars show mean ± SD of three technical replicates of three independent experiments (unpaired Student's *t*-test). ChIP, chromatin immunoprecipitation.

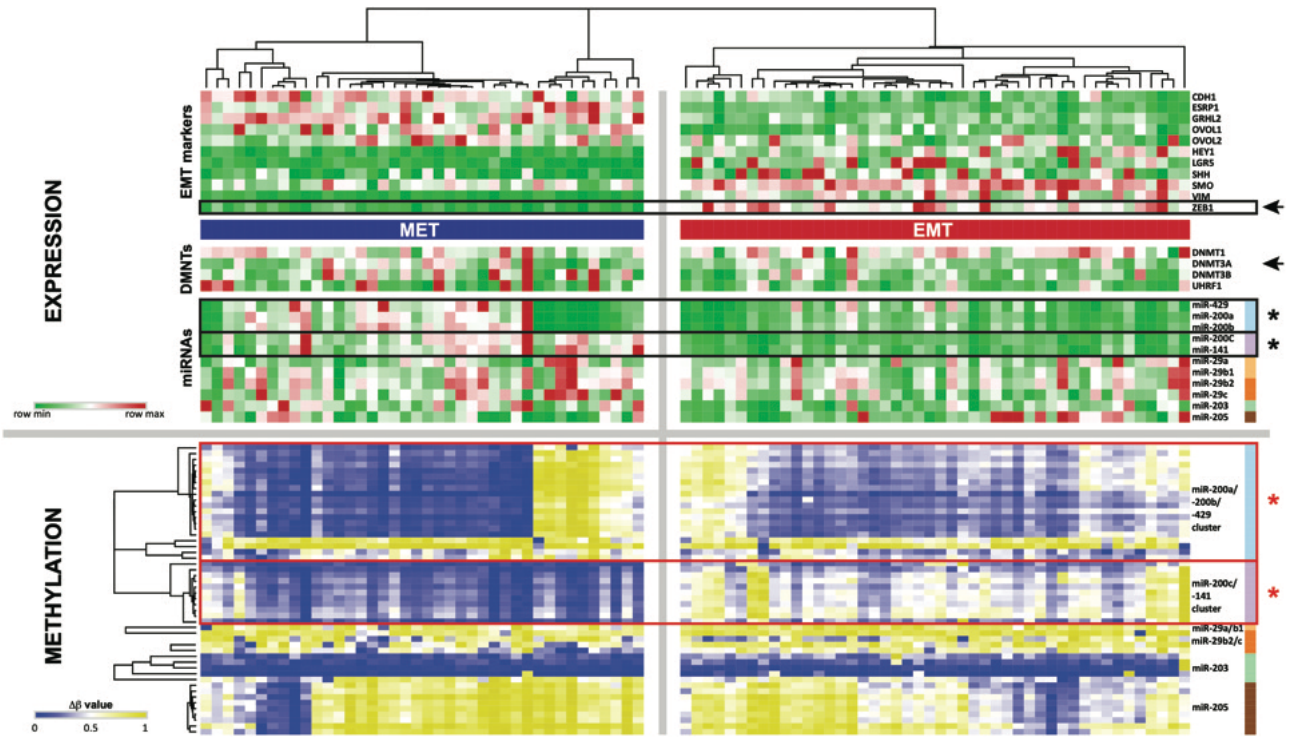

Figure 3. Alteration of the miRNome in PCa patients (PRAD-TCGA dataset). A primary prostate adenocarcinoma (TCGA-PRAD) dataset containing 494 patients was enquired (https://gdc-portal.nci.nih.gov). IlluminaHiSeq mRNA-Seq expression data were used to classify patients; each patient was assigned to the EMT-like category when EMT genes were expressed at high levels (>Q3 or Q4) and MET genes at low levels (<Q1 or Q2), or to the MET-like category when displaying the opposite signature (see Materials and methods). Patients showing positive scores for EMT- or MET-like profiles were chosen (47 and 40 cases, respectively); the heatmap shows the expression of the EMT genes and of DNMTs (IlluminaHiSeq), and the comparison between miRNA expression (IlluminaHiSeq) and cytosines DNA methylation (Illumina Infinium, HumanMethylation 450 array) of the miRNAs found DE and methylated in CM-CAFs versus CM-HFPs PC3 cells (black/red boxes: expression/methylation of miRNAs; arrows: expression of ZEB1 and DNMT3A).

Identification of potential miRNA regulators of DNMT3A in EMT

To further explore the mechanisms behind the regulation of DNMT3A protein levels during *ex vivo* EMT, we examined the involvement of the miRNA-mediated regulation of *DNMT3A* mRNA. DNMT3A is a known target of various miRNAs, in particular the miR-29 family (23). We previously demonstrated that all three miRNAs of the -29 cluster (miR-29a, -29b and -29c) are down-regulated during *ex vivo* EMT (6). Contrary to what previously assessed via qPCR, despite a reduction in read counts for miR-29a and miR-29b, their down-regulation resulted not statistically significant in our RNA seq (Supplementary Figure 2A, available at *Carcinogenesis* Online).

Therefore, we set to identify new potential DNMT3A regulators among the DE miRNAs. By enquiring multiple *in silico* tools, we produced a list of miRNAs identified by at least two tools that was used to isolate potential interactors of *DNMT3A* mRNA among our DE miRNAs. The analysis revealed a list of 10 up-regulated and 8 down-regulated miRNAs (Supplementary Table 2A and B, available at *Carcinogenesis* Online, grey boxes). Among the down-regulated ones, our attention focussed on miR-429 and miR-200b, as they are regulated by DNMT3A and contain a shared a seeding sequence directed to its 3′UTR. Conversely, among up-regulated miRNAs we noticed miR-1260a, that so far has not been linked to DNMT3A and that we previously found altered in UHRF1-silenced PC3 cells, where it resulted significantly up-regulated in combination with DNMT3A down-regulation (Supplementary Figure 2C, available at *Carcinogenesis* Online).

Our data show that, during *ex vivo* EMT, DNMT3A is epigenetically regulated not only via promoter methylation, as previously published (6), but potentially also by miRNome alteration, as several deregulated miRNAs are identified by *in silico* analysis as potentially targeting *DNMT3A*-3′UTR. In particular, the down-regulated miR-200b/429 and the up-regulated miR-1260a represent the most interesting potential interactors of DNMT3A.

Validation of miR-1260a and miR-429 as regulators of *DNMT3A* mRNA and assessment of a feedback loop between miR-200b/429 and DNMT3A in EMT

There is no current evidence in the literature about possible roles for miR-1260a or its interactors in cancer progression, while miR-200b and miR-429 have been extensively investigated (40,43). In particular, miR-200b has already been demonstrated to directly target DNMT3A in ovarian cancer (40), while the ability of miR-429 to target it is only speculated. We first assessed miR-1260a, miR-200b and miR-429 expression in our *ex vivo* EMT model and in different PCa cell lines. We observed a significant reduction of all three miRNAs in CM-CAFs compared with CM-HPFs (Figure 4A, left panel); for miR-1260a, this result is in contrast with the RNA-Seq analysis (Supplementary Table 2B, available at *Carcinogenesis* Online). In LNCaP and PC3 non-treated cells, *DNMT3A* mRNA levels show an inverse trend with the expression of miR-1260a, miR-200b and miR-429: lower levels of *DNMT3A* mRNA and higher amounts of miRNAs were detected in LNCaP, and *vice versa* in PC3 (Figure 4A, right panel, and Supplementary Figure 2B, available at *Carcinogenesis* Online).

Inspection of *DNMT3A*-3′UTR by accessibility analysis (37) identified two seed sites for miR-1260a and one for miR-429, shared with miR-200b (Supplementary Figure 3A, available at *Carcinogenesis* Online). To verify the ability of these miRNAs to

target *DNMT3A*-3′UTR, we co-transfected the pGL4.13-*DNMT3A*-3′UTR plasmid along with miR-1260a or miR-429 overexpressing plasmid (psiUx-miR-1260a, psiUx-miR-429) in PC3-NT cells. We did not test miR-200b as it has already been shown to target *DNMT3A* 3′UTR (40). psiUx-miR-608 and psiUx-miR-29a were used as negative and positive control, respectively, as no binding sites for miR-608 are known or predicted on *DNMT3A*-3′UTR, while miR-29a directly targets *DNMT3A*-3′UTR (23). psiUx-miR-1260a and psiUx-miR-429 reduced luciferase activity of about 40% and 30% relative to psiUx-miR-608, respectively (Figure 4B and Supplementary Figure 3C, available at *Carcinogenesis* Online), suggesting a direct binding on *DNMT3A*-3′UTR. psiUx-miR-29a led to a 25% decrease in luciferase activity, as expected (Figure 4B). These results prove the ability of miR-429 to target DNMT3A and confirm previous data for miR-200b. To support the specificity of miR-1260a binding, we co-transfected *DNMT3A*-3′UTR deletion mutants (Δ1260a_1, Δ1260a_2 and the double mutant Δ1260a_1_2) with psiUx-miR-1260a or psiUx-miR-608. No reduction of luciferase activity was detected upon co-transfection of psiUx-miR-1260a with Δ1260a_1_2 constructs, while a reduction was observed with the Δ1260a_1 and Δ1260a_2 mutants, separately (Supplementary Figure 3C, available at *Carcinogenesis* Online), indicating the both sites targeted by miR-1260a contribute to its activity.

Furthermore, we characterized the effects of the overexpression/down-regulation of these miRNAs on DNMT3A levels and EMT factors. Given the statistically different (higher) levels of both miRNAs in LNCaP versus PC3, corresponding to an opposite trend in DNMT3A expression levels (Figure 4A), we performed mimicry in PC3 and inhibition in LNCaP, to evaluate the impact of the differential manipulations in the two cell lines. Both mimic-1260a and mimic-429 reduced DNMT3A mRNA and protein levels in PC3-NT, while miRNA inhibitors slightly increased them in LNCaP (Figure 4C and D, left). miR-429 deregulation appears to affect mostly DNMT3A1 isoform, while miR-1260a affects the two isoforms equally, and to a greater extent compared with miR-429. Since the 3′UTR is identical in both isoforms, this preference could be ascribed to secondary mechanisms linked to miR-429 variations. Concerning EMT factors (Figure 4C and D, right panel, and Supplementary Figure 4A and B, available at *Carcinogenesis* Online), miR-429 had a very strong impact on all the analysed factors, in particular ZEB1, confirming the importance of this miRNA for the transition. Conversely, the contribution of miR-1260a on EMT gene expression/protein levels resulted less evident.

Finally, we assessed whether cell growth and migration ability were also affected by the deregulation of the miRNAs. In PC3 cells, only miR-1260a mimic significantly reduced cell proliferation after 5 days (Figure 5A, left). Instead, miR-429 mimic strongly inhibited cell migration, with greater efficacy than miR-1260a mimic (Figure 5A, right panel). In LNCaP cells, inhibition of both miRNAs did not affect cell proliferation, while only LNA-429 mildly increased cell migration (Figure 5B, left panel). Taken together, these data argue in favour of a role of miR-429, but not of miR-1260a, on cell migration by affecting several genes involved in the EMT, rather than on cell proliferation.

Previous assessment of miR-429 and miR-200b behaviour in the PRAD patients' dataset (Figure 3) showed an inverse correlation of the expression of these miRNAs with the EMT phenotype. Conversely, miR-1260a expression was detectable only in 12 tumour samples, among which only one was present in the EMT- and MET-like clusters (Supplementary Figure 4C, available at *Carcinogenesis* Online). miR-1260a locus methylation levels did not show any evident correlation with its expression.

In conclusion, miR-1260a can directly regulate *DNMT3A*, and its modulation significantly alters DNMT3A levels in PC3 and LNCaP cells; however, this miRNA is not abundantly expressed in PCa patients and does not seem to be a direct player in the EMT. Conversely, the feedback loop between miR-200b/-429 and DNMT3A, and the concomitant action on EMT factors such as ZEB1 underline the importance of these two miRNAs for the EMT process in PCa.

Discussion

In this study, we provide strong evidence that the interplay of DNMT3A with several miRNAs has a central role in the EMT occurring during PCa progression. We identified a feedback loop between miR-429 and DNMT3A that promotes and sustains the transition towards a more mesenchymal phenotype, and we hypothesize that this is likely supported by the differential expression of two DNMT3A isoforms (a and b) during the process.

EMT is an intrinsic metastable process, susceptible to undergo the reverse MET according to the stimuli conveyed. The relevance of the molecular signals from local microenvironment and cancer-associated stroma in the induction and functional activation of the EMT and the reverse MET pathways has been greatly explored in the last decade (24,44,45); TGFβ is the most investigated player, although other factors generated from the neighbouring tumour microenvironment contribute to the process. Consistent with its inherent plasticity, it has been hypothesized that epigenetic events have crucial functions in triggering and establishing the intermediate and final phenotype. In support of this view, we previously demonstrated that reversible DNA methylation alterations are pivotal during the EMT–MET program in PCa, resulting in transcriptome rewiring (6). In this context, we showed that DNMT3A induces reversible methylome changes in PC3 cells, but not in LNCaP cells, following exposure to patient-derived cancer-associated fibroblasts conditioned medium (6). We report here that microenvironmental stimuli also induce the epigenetic switches on miRNA promoters, and that DNMT3A is the putative regulator of the DNA methylation variations occurring at various miRNA promoters in our *ex vivo* model system. We especially focussed on the promoter regions showing *de novo-methylation*, as we were interested in highlighting the interplay between DNMT3A and miRNAs in the transition. Indeed, miR-200c and miR-141, two of the best-known and studied miRNA regulated by DNA methylation in PCa, have been reported to control DNMT3A expression (42). The chromatin immunoprecipitation data presented here confirm that DNMT3A binds to the promoter region and epigenetically regulates the miR-200 family (miR-200a/200b/429 and miR-200c/141), miR-203 and miR-205 loci. DNMT1 also binds to these promoters, suggesting its involvement in the maintenance of the newly deposited methylation on miR-203, miR-200b/200b/429 and miR-205, while it is already present on miR-200c/141, as expected by the high DNA methylation level detected in HPF samples. Our results further highlight the role of DNMT3A in altering the expression of several onco-suppressors miRNAs, which include among others miR-639 in liver cancer cells (46) and miR-105 in gastric cancer (47).

The relevance of the epigenetic control of miRNA expression during EMT was further confirmed by analysing the miRNA database of the TCGA dataset, selecting only those samples having a clearly defined EMT/MET expression signature, and comparing the methylation profile with the miRNA expression data. In 86 evaluated patients, we detected an inverse correlation between the expression of EMT factors, such as ZEB1, and

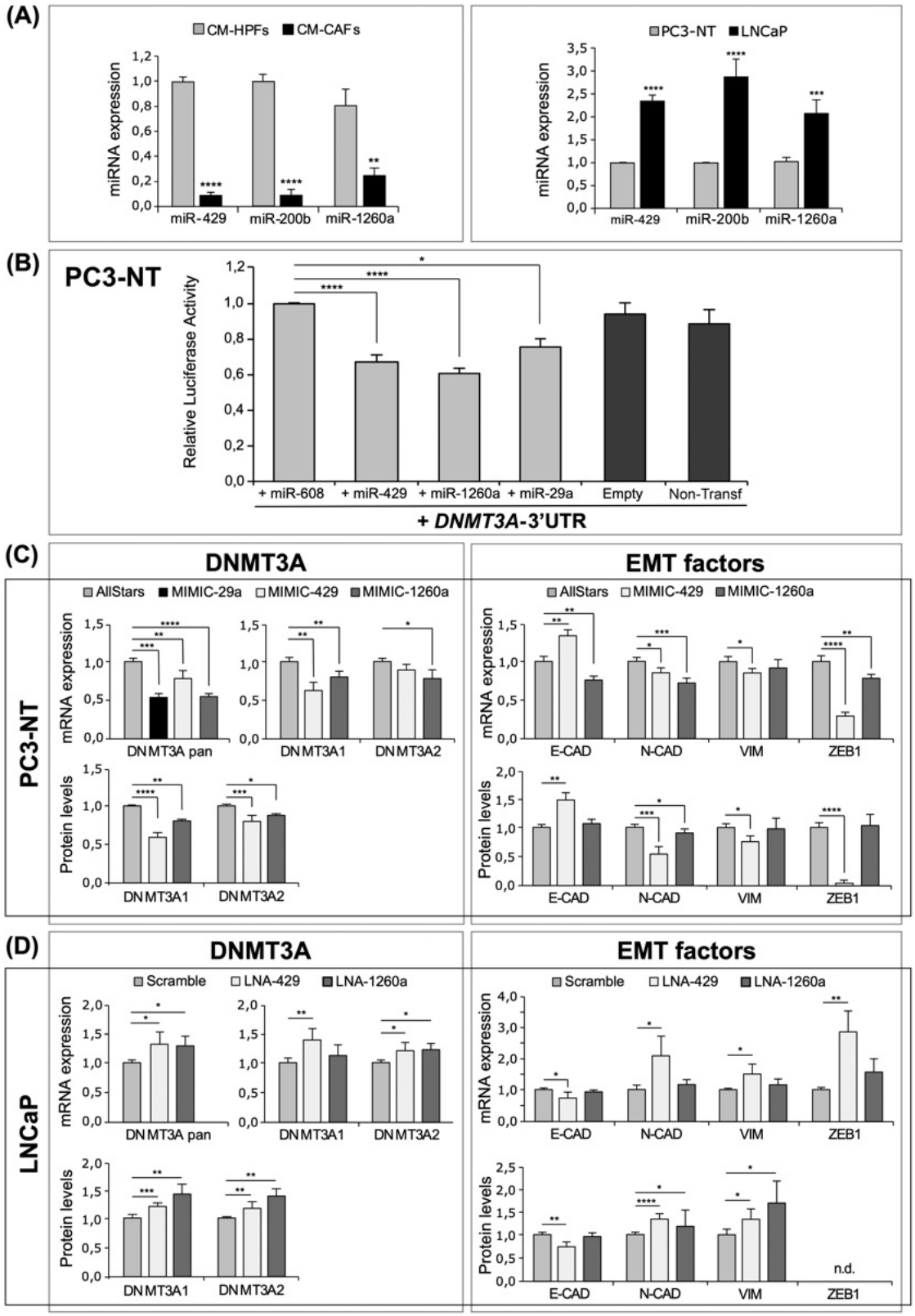

Figure 4. Identification and validation of new potential *DNMT3A* regulators among miRNAs altered during *ex vivo* EMT. (**A**) Evaluation of miR-200b, miR-429 and miR-1260a expression levels during EMT and in PCa cell lines. Transcriptional levels of the three miRNAs were assessed in CM-CAFs versus CM-HPFs PC3 cells and in LNCaP versus PC3-NT (non-treated) cells. miRNA expression was compared with DNMT3A (pan) expression levels in the same cells. (**B**) Functional analysis of miR-429 and miR-1260a binding to *DNMT3A* 3′UTR. *DNMT3A*-3′UTR was cloned downstream of the Firefly luciferase gene in pGL4.13 plasmid and co-transfected in PC3-NT cells with plasmids overexpressing miR-429 or miR-1260a. miR-608 was used as negative control, miR-29a/b as positive control. Empty = transfected with psiUx-empty; Non-Transf = non-transfected cells (*DNMT3A*-3′UTR only) ($N = 3$; Student's *t*-test). (**C** and **D**) Characterization of miR-429 and miR-1260a overexpression/down-regulation in PCa cell lines. (Left) DNMT3A variations in PC3-NT cells transfected with MIMIC oligos (C) and in LNCaP cells transfected with LNA-inhibitor oligos (C) were evaluated both at mRNA and protein levels. (Right) Alteration of the transcriptional and protein levels of key EMT factors was evaluated following miR-429/miR-1260a mimicry in PC3-NT cells and miR-429/miR-1260a inhibition in LNCaP cells. n.d. = not detected ($N = 4$; Student's *t*-test) (*$P \leq 0.05$, **$P \leq 0.01$, ***$P \leq 0.001$, ****$P \leq 0.0001$).

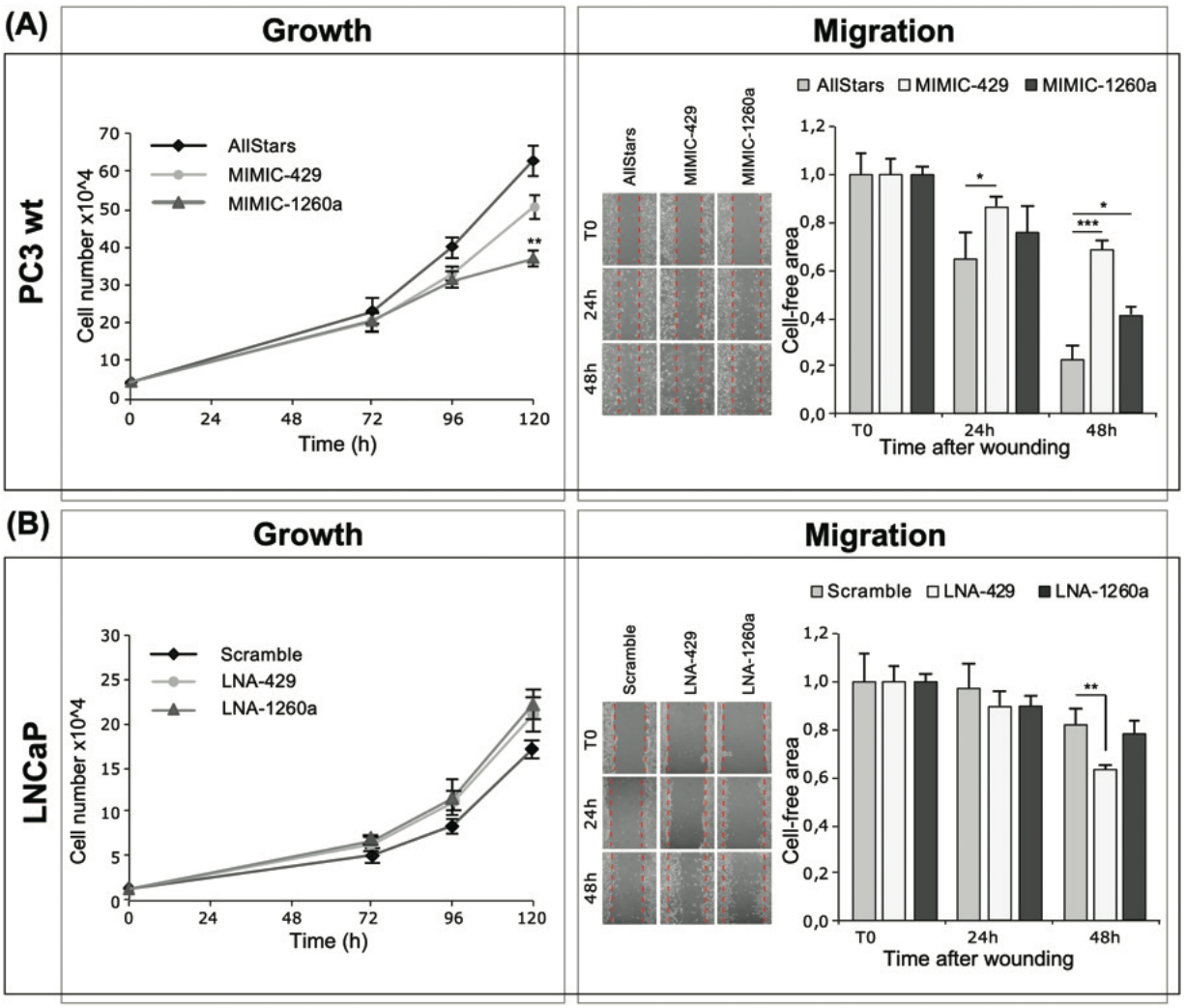

Figure 5. Phenotypic alterations following miR-429 or miR-1260a overexpression/down-regulation. (**A**) Proliferation and migration ability of PC3-NT cells after miR-429 or miR-1260a ectopic expression. Cell growth curve (left), and wound-healing assays (right) after mimics transfection. (**B**) Proliferation and migration of LNCaP cells after inhibition of miR-429 or miR-1260a. Cell growth curve (left) and wound-healing assays (right) after LNA-inhibitors transfection. Pictures were taken at T0, 24 h and 48 h after monolayer wounding; cell growth was assessed at the same time points. Cell migration is shown as means values ± SDs of the measurements of the cell-free area for each time point and condition. Each experiment was performed in triplicate (one-way ANOVA test). Pictures shown are representative of the average behaviour.

onco-suppressor miRNAs, such as miR-200c/miR-141, coupled with a strong alteration in DNA methylation, in accordance with the results from our experimental model. miR-200a/200b/429 display a strong correspondence between 5-mC levels on promoter and expression, suggesting a direct control of DNA methylation on their expression. It is worth noting that a cluster of MET-like patients, presenting an epithelial signature, show very low levels of these miRNAs. DNA methylation seems to have a relevant role in the control of miR-205 expression, but not of miR-203 *in vivo*, although miR-205, differently from our experimental setting, it is not related to the EMT/MET conditions. Altogether, our data further sustain the requirement of DNMT3A for EMT achieved by modulating the expression of a series of miRNAs involved in this process.

This study strongly supports the pivotal role of the interplay between DNMT3A and several miRNAs in EMT and, ultimately, in PCa progression. DNMT3A itself is a target of miRNAs; its expression, indeed, is regulated by at least miR-29 (23), miR-143 (48) and miR-200b (40). In particular, we show a feedback loop between miR-429 and DNMT3A which strongly directs cancer cells towards a more mesenchymal phenotype. While these two miRNAs have already been separately linked to EMT or DNMTs regulation in various tumours (32,40), here we assess the importance of the interplay between these factors in the transition, as well as the ability of miR-429 to directly target DNMT3A. Feedback loops between DNMT3A and miRNAs have already been demonstrated in various cancers; the DNMT3A/miR-200c loop has a relevant role during carcinogenesis and progression in gastric cancer (49), while a negative feedback between miR-143 and DNMT3A regulates cisplatin resistance in ovarian cancer (50). Altogether, these findings strongly support the idea that DNMT3A and specific miRNAs work through feedback loops to regulate important biological processes relevant to cancer, such as EMT.

miR-1260a was also identified as a novel interactor of DNMT3A potentially involved in the EMT–MET pathway. This miRNA strongly impacts DNMT3A expression, as we observed an inverse correlation between its levels and DNMT3A expression in our *ex vivo* model and in PCa cell lines. Its effects on the EMT factors, however, are not as prominent; our data support the hypothesis that during PCa progression the DNMT3A–miR1260a axis could be implicated in cell growth more than in

the EMT process. However, investigation of the TCGA dataset resulted in the recognition of few patients expressing miR-1260a. On the basis of these data, we conclude that, despite being established as a true interactor of DNMT3A *in silico* and *in vitro*, miR-1260a is not abundantly expressed in PCa patients' samples and therefore is not a fundamental player in PCa progression.

Elucidation of the complete profile of DNA methylation alterations at miRNA promoters, and the identification of feedback loops between miRNAs and DNMTs, could provide a diagnostically/prognostically significant signature for prostatic cancer patients, especially for recognizing and monitoring the progression towards more aggressive traits.

Supplementary material

Supplementary data are available at *Carcinogenesis* online.

Funding

EPIGEN Flagship Project (EPIGEN-CNR-IT) to I.M.B., A.W. and L.S.; Italian Association for Cancer Research (IG-23068) and Regione Campania (POR Campania FESR 2014/2020, azione 1.5, CUP:B41C17000080007) to A.W.; EU H2020 MSCA-RISE project diaRNAgnosis (101007934), Fondazione CARITRO and University of Trento, Department CIBIO to M.A.D.
Conflict of Interest Statement: None declared.

Ethical approval

The study named 'Ruolo del microambiente stromale nella immunomodulazione e nella progressione del carcinoma prostatico (Role of the stromal microenvironment for immunomodulation and for cancer progression in prostatic carcinoma)' was approved by the Ethics committee 'Area Vasta Centro' (Azienda Ospedaliera Universitaria Careggi, Florence, Italy) with reference number 'BIO15.016' (26.06.2015).

Data availability

Raw DNA methylation microarray data and raw coding RNA sequencing data have been previously deposited in the EBI ArrayExpress Database (https://www.ebi.ac.uk/arrayexpress/) (6) with accession numbers E-MTAB-4753 and E-MTAB-4752, the raw noncoding RNA sequencing data have been deposited in the EBI ArrayExpress Database with accession number E-MTAB-9835 and the Agilent microarray data are available at NCBI's Gene Expression Omnibus (GEO) (https://www.ncbi.nlm.nih.gov/geo) under accession number GSE162719.

References

1. Ferlay, J. *et al.* (2018) Cancer incidence and mortality patterns in Europe: estimates for 40 countries and 25 major cancers in 2018. *Eur. J. Cancer*, 103, 356–387.
2. Siegel, R.L. *et al.* (2018) Cancer statistics, 2018. *CA Cancer J. Clin.*, 68, 7–30.
3. Angeles, A.K. *et al.* (2018) Genome-based classification and therapy of prostate cancer. *Diagnostics (Basel)*, 8, 62–88.
4. Lo, U.G. *et al.* (2017) The role and mechanism of epithelial-to-mesenchymal transition in prostate cancer progression. *Int. J. Mol. Sci.*, 18, 2079–2097.
5. Nieto, M.A. *et al.* (2016) EMT: 2016. *Cell*, 166, 21–45.
6. Pistore, C. *et al.* (2017) DNA methylation variations are required for epithelial-to-mesenchymal transition induced by cancer-associated fibroblasts in prostate cancer cells. *Oncogene*, 36, 5551–5566.
7. Baylin, S.B. *et al.* (2011) A decade of exploring the cancer epigenome—biological and translational implications. *Nat. Rev. Cancer*, 11, 726–734.
8. Heyn, H. *et al.* (2012) DNA methylation profiling in the clinic: applications and challenges. *Nat. Rev. Genet.*, 13, 679–692.
9. Paziewska, A. *et al.* (2014) DNA methylation status is more reliable than gene expression at detecting cancer in prostate biopsy. *Br. J. Cancer*, 111, 781–789.
10. Ashraf, W. *et al.* (2017) The epigenetic integrator UHRF1: on the road to become a universal biomarker for cancer. *Oncotarget*, 8, 51946–51962.
11. Angulo, J.C. *et al.* (2016) Development of castration resistant prostate cancer can be predicted by a DNA hypermethylation profile. *J. Urol.*, 195, 619–626.
12. Ellinger, J. *et al.* (2008) CpG island hypermethylation at multiple gene sites in diagnosis and prognosis of prostate cancer. *Urology*, 71, 161–167.
13. Massie, C.E. *et al.* (2017) The importance of DNA methylation in prostate cancer development. *J. Steroid Biochem. Mol. Biol.*, 166, 1–15.
14. Qin, W. *et al.* (2015) DNA methylation requires a DNMT1 ubiquitin interacting motif (UIM) and histone ubiquitination. *Cell Res.*, 25, 911–929.
15. Lyko, F. (2018) The DNA methyltransferase family: a versatile toolkit for epigenetic regulation. *Nat. Rev. Genet.*, 19, 81–92.
16. Lin, R.K. *et al.* (2014) Dysregulated transcriptional and post-translational control of DNA methyltransferases in cancer. *Cell Biosci.*, 4, 57.
17. Gravina, G.L. *et al.* (2013) Increased levels of DNA methyltransferases are associated with the tumorigenic capacity of prostate cancer cells. *Oncol. Rep.*, 29, 1189–1195.
18. Gravina, G.L. *et al.* (2011) Hormonal therapy promotes hormone-resistant phenotype by increasing DNMT activity and expression in prostate cancer models. *Endocrinology*, 152, 4550–4561.
19. Wahid, F. *et al.* (2010) MicroRNAs: synthesis, mechanism, function, and recent clinical trials. *Biochim. Biophys. Acta*, 1803, 1231–1243.
20. Peng, Y. *et al.* (2016) The role of MicroRNAs in human cancer. *Signal Transduct. Target. Ther.*, 1, 1–9.
21. Sharma, N. *et al.* (2018) The microRNA signatures: aberrantly expressed miRNAs in prostate cancer. *Clin. Transl. Oncol*, 21, 126–144.
22. Bryzgunova, O.E. *et al.* (2018) MicroRNA-guided gene expression in prostate cancer: literature and database overview. *J. Gene Med.*, 20, e3016.
23. Morita, S. *et al.* (2013) miR-29 represses the activities of DNA methyltransferases and DNA demethylases. *Int. J. Mol. Sci.*, 14, 14647–14658.
24. Davalos, V. *et al.* (2012) Dynamic epigenetic regulation of the microRNA-200 family mediates epithelial and mesenchymal transitions in human tumorigenesis. *Oncogene*, 31, 2062–2074.
25. Lin, S. *et al.* (2015) MicroRNA biogenesis pathways in cancer. *Nat. Rev. Cancer*, 15, 321–333.
26. Ramassone, A. *et al.* (2018) Epigenetics and microRNAs in cancer. *Int. J. Mol. Sci.*, 19, 459–487.
27. Saini, S. *et al.* (2011) Regulatory role of mir-203 in prostate cancer progression and metastasis. *Clin. Cancer Res.*, 17, 5287–5298.
28. Kalogirou, C. *et al.* (2013) MiR-205 is progressively down-regulated in lymph node metastasis but fails as a prognostic biomarker in high-risk prostate cancer. *Int. J. Mol. Sci.*, 14, 21414–21434.
29. Ru, P. *et al.* (2012) miRNA-29b suppresses prostate cancer metastasis by regulating epithelial-mesenchymal transition signaling. *Mol. Cancer Ther.*, 11, 1166–1173.
30. Pieraccioli, M. *et al.* (2013) Activation of miR200 by c-Myb depends on ZEB1 expression and miR200 promoter methylation. *Cell Cycle*, 12, 2309–2320.
31. Bracken, C.P. *et al.* (2008) A double-negative feedback loop between ZEB1-SIP1 and the microRNA-200 family regulates epithelial-mesenchymal transition. *Cancer Res.*, 68, 7846–7854.
32. Gregory, P.A. *et al.* (2008) The miR-200 family and miR-205 regulate epithelial to mesenchymal transition by targeting ZEB1 and SIP1. *Nat. Cell Biol.*, 10, 593–601.
33. Chen, Y. *et al.* (2020) miRDB: an online database for prediction of functional microRNA targets. *Nucleic Acids Res.*, 48, D127–D131.
34. Agarwal, V. *et al.* (2015) Predicting effective microRNA target sites in mammalian mRNAs. *eLife*, 4, e05005.
35. Oulas, A. *et al.* (2012) A new microRNA target prediction tool identifies a novel interaction of a putative miRNA with CCND2. *RNA Biol.*, 9, 1196–1207.
36. Pio, G. *et al.* (2015) ComiRNet: a web-based system for the analysis of miRNA-gene regulatory networks. *BMC Bioinformatics*, 16 (suppl. 9), S7.
37. Kertesz, M. *et al.* (2007) The role of site accessibility in microRNA target recognition. *Nat. Genet.*, 39, 1278–1284.

38. Rehmsmeier, M. *et al*. (2004) Fast and effective prediction of microRNA/target duplexes. *RNA*, 10, 1507–1517.
39. Denti, M.A. *et al*. (2004) A new vector, based on the PolII promoter of the U1 snRNA gene, for the expression of siRNAs in mammalian cells. *Mol. Ther.*, 10, 191–199.
40. Liu, J. *et al*. (2019) miR-200b and miR-200c co-contribute to the cisplatin sensitivity of ovarian cancer cells by targeting DNA methyltransferases. *Oncol. Lett.*, 17, 1453–1460.
41. Fang, H. *et al*. (2009) ArrayTrack: an FDA and public genomic tool. *Methods Mol. Biol.*, 563, 379–398.
42. Lynch, S.M. *et al*. (2016) Regulation of miR-200c and miR-141 by methylation in prostate cancer. *Prostate*, 76, 1146–1159.
43. Guo, C.M. *et al*. (2020) miR-429 as biomarker for diagnosis, treatment and prognosis of cancers and its potential action mechanisms: a systematic literature review. *Neoplasma*, 67, 215–228.
44. Pardali, K. *et al*. (2007) Actions of TGF-beta as tumor suppressor and pro-metastatic factor in human cancer. *Biochim. Biophys. Acta*, 1775, 21–62.
45. Xu, J. *et al*. (2009) TGF-beta-induced epithelial to mesenchymal transition. *Cell Res.*, 19, 156–172.
46. Xiao, J. *et al*. (2020) miR-639 expression is silenced by DNMT3A-mediated hypermethylation and functions as a tumor suppressor in liver cancer cells. *Mol. Ther.*, 28, 587–598.
47. Zhou, G.Q. *et al*. (2017) DNMT3A-mediated down-regulation of microRNA-105 promotes gastric cancer cell proliferation. *Eur. Rev. Med. Pharmacol. Sci.*, 21, 3377–3383.
48. Karimi, L. *et al*. (2017) Function of microRNA-143 in different signal pathways in cancer: new insights into cancer therapy. *Biomed. Pharmacother.*, 91, 121–131.
49. Li, Y. *et al*. (2016) Epigenetically deregulated miR-200c is involved in a negative feedback loop with DNMT3a in gastric cancer cells. *Oncol. Rep.*, 36, 2108–2116.
50. Han, X. *et al*. (2021) The negative feedback between miR-143 and DNMT3A regulates cisplatin resistance in ovarian cancer. *Cell Biol. Int.*, 45, 227–237.